NACA RM L57E28

NACA

RESEARCH MEMORANDUM

ANALYSIS OF WING LOADS MEASURED ON A FLEXIBLE SWEPT-WING JET BOMBER DURING PUSH-PULL MANEUVERS

By Patrick A. Gainer and Paul W. Harper

Langley Aeronautical Laboratory
Langley Field, Va.

NATIONAL ADVISORY COMMITTEE
FOR AERONAUTICS

WASHINGTON

July 23, 1957
Declassified October 8, 1957

NATIONAL ADVISORY COMMITTEE FOR AERONAUTICS

RESEARCH MEMORANDUM

ANALYSIS OF WING LOADS MEASURED ON A FLEXIBLE SWEPT-WING JET BOMBER DURING PUSH-PULL MANEUVERS

By Patrick A. Gainer and Paul W. Harper

SUMMARY

Loads on the wing of a Boeing B-47A medium bomber were measured by means of strain-gage instrumentation during 23 gradual symmetrical push-pull maneuvers performed at altitudes from 15,000 to 30,000 feet, Mach numbers from 0.47 to 0.81, and gross weights from 105,500 to 114,500 pounds. These measurements, together with supplementary measurements of load factor and other flight parameters, were reduced in order to obtain time histories of aerodynamic shear, bending moment, and torque at each of four spanwise stations on the left wing and at one station on the right wing. These time histories were analyzed in order to determine additional and basic load components for the purpose of checking currently available methods of predicting loadings on flexible wings.

From the comparison of experimental and theoretical results, it is concluded that presently available methods are capable of predicting additional and basic loads accurately within the range of flight conditions covered by the tests.

INTRODUCTION

The quantitative checking, by load measurements in flight, of the loads predicted by available calculation procedures continues to be of importance, particularly for the case where large interference and flexibility effects exist. The National Advisory Committee for Aeronautics has recently completed a program in which deflections and loads over various parts of the relatively flexible Boeing B-47A airplane were measured for the specific purpose of providing such data.

Some phases of this program have been reported in references 1 to 4. In the present report the primary consideration is with that phase of the program dealing with the measurements of the shear, bending moment, and torque at a number of stations across the wing span and the comparison

of these results with those predicted by applicable engineering methods. The data for this report were obtained during symmetrical push-pull maneuvers performed at a slow rate so that quasi-static conditions prevailed. The maneuvers covered a Mach number range from 0.47 to 0.81, an altitude range from 15,000 to 30,000 feet, and a gross airplane weight range of 105,500 to 114,500 pounds.

SYMBOLS

b	wing span, in.
L_T	horizontal-tail aerodynamic load, lb
m_R	lift-curve slope of the rigid airplane without the tail, per deg
M	Mach number
n	normal load factor at airplane center of gravity, g units
q	dynamic pressure, lb/sq ft
S	wing area, sq ft
F_s	aerodynamic shear force, positive for up load, lb
M_b	aerodynamic bending moment, positive for up load, in-lb
T	aerodynamic torque, negative for up load rearward of strain-gage reference station, in-lb
W	airplane gross weight, lb
x	coordinate measured from intersection of wing front spar and airplane center line, parallel to center line, positive forward, in.
y	coordinate measured from intersection of wing front spar and center line, perpendicular to center line, positive outboard, in.
x'	streamwise distance from a strain-gage reference station to the center of pressure of the additional airload carried outboard of the station, in.

y' spanwise distance from strain-gage reference station to the center of pressure of the additional airload carried outboard of the station, in.

α_0 wing-root angle of attack at zero lift, measured at center line, deg

α_r wing-root angle of attack measured at center line, deg

Λ sweep angle of wing quarter-chord line, deg

$\dot{\theta}$ pitching angular velocity, radians/sec

$\ddot{\theta}$ pitching angular acceleration, radians/sec^2

Subscripts:

add due to additional load

av average

cl referred to the airplane center line

0 at zero load factor

sta referred to a strain-gage station

APPARATUS AND TESTS

A standard B-47A medium bomber was used to obtain the test data analyzed in this report. The only external modifications consisted of the addition of a faired nose boom containing the airspeed head and the angle-of-attack and sideslip vanes, and the addition of a housing for the optigraph (deflection recording) cameras rearward of the cockpit canopy. These additions were not considered to cause any appreciable load-distribution changes. Figure 1 is a photograph of the test airplane. A three-view drawing showing the modifications is given in figure 2. Pertinent physical characteristics of the airplane are given in table I.

Instrumentation

NACA standard instruments were used to record airspeed, altitude, fuselage angle of attack, rotational velocities and accelerations, linear accelerations, and control-surface displacements. The distribution of

the normal load factor along the wing span was measured by means of remotely recording accelerometers, located as shown in the plan-form view of figure 3. Normal and transverse load factors at the nacelles were also recorded.

Electrical wire resistance strain gages were mounted at four spanwise stations on the left wing, at one station on the right wing, on the engine nacelle struts, and at the horizontal-tail root. The reference points for the wing gage stations were located on the front spar at 7.8, 36.2, 59.5, and 82.2 percent of the semispan on the left wing and at 7.8 percent on the right wing. The gages for each station were calibrated by the methods described in reference 5. Equations were obtained from the calibrations to give, in terms of bridge outputs, the structural shear at each reference station and the structural bending moment and torque about the reference axes at each station. The bending-moment axes were parallel to the airplane center line, and the torque axis for each station was perpendicular to the corresponding bending-moment axis. The bridge outputs were recorded in flight on multichannel oscillographs.

Loads applied to the inboard engine nacelle produced some localized twisting of the front spar and thereby affected the responses of the strain gages in the wing at 36.2 percent semispan. Errors in the wing-plus-nacelle shear, bending moment, and torque measured at this station were found to be proportional to the nacelle structural pitching moment. Provision was, therefore, made for correcting these errors by using the measured nacelle pitching moment.

Tests

The maneuvers analyzed for this report (runs 5 to 27 of flight 25 of the general test program) consisted of 23 push-pull or roller-coaster maneuvers performed at Mach numbers up to 0.81 and altitudes from 15,000 to 30,000 feet. The gross airplane weight during these maneuvers varied from 105,500 to 114,500 pounds. All fuel was carried in the fuselage. All pertinent quantities were recorded continuously during each run.

The maneuvers used for the analysis covered the Mach number range in such a way that the Mach numbers were repeated at each of four altitudes, except that a Mach number of 0.81 could not be attained at the lowest altitude (15,000 feet) because of the 425-knot placard speed.

The gradualness of the maneuvers used was desirable for minimizing the effects of pitching acceleration, and because of this gradualness some changes in dynamic pressure and Mach number occurred in each run.

Table II gives the flight conditions, including the average, the maximum, and the minimum dynamic pressure and Mach number for each of the 23 runs analyzed.

METHOD AND RESULTS

For the maneuvers listed in table II, time histories were recorded of structural shear, bending moment, and torque at the four wing stations. Time histories were also recorded of all other pertinent loading parameters such as load factors, dynamic pressure, Mach number, pitching velocity, and acceleration.

Time histories of aerodynamic shear, bending moment, or torque at any wing strain-gage station were obtained by adding the measured inertia component to the measured structural loading component. The structural component was determined from the strain-gage-bridge outputs by use of the calibration equations. The inertia component was obtained from the known dead-weight distribution of the wing and the time histories of the measured load-factor distribution.

The measured loadings at the 36.2-percent-semispan station were to be corrected for local strain distortions caused by inboard-nacelle airload and inertia load. As stated previously, the intention was that the strain gages on the nacelle strut be used for determining these corrections at the 36.2-percent-semispan station. The nacelle strain gages failed to operate satisfactorily in flight, and it was therefore necessary to base the corrections on the nacelle inertia load alone. Neglect of the nacelle airload may have contributed a maximum error of about 3 percent to the additional aerodynamic loads at the 36.2-percent station.

Failure of the nacelle strain gages also made it impossible to determine separate wing and nacelle aerodynamic loadings; therefore, the aerodynamic quantities presented in this report are wing-plus-nacelles values.

Analysis of Time Histories

In the analysis, the aerodynamic-load time histories were considered to consist of basic and additional load components as well as possible minor load components caused by pitching velocity and pitching acceleration. The basic load components are those at zero normal load factor for the airplane, zero pitching velocity, and zero pitching acceleration. The additional component is the increment in loading per unit change in airplane normal load factor alone. For this report the primary objective

was to determine the basic and additional components of wing shear, bending moment, and torque at each station.

Provided dynamic pressure and Mach number are constant, the following equations describe the aerodynamic loadings at each station in terms of load factor n, pitching velocity $\dot{\theta}$, and pitching acceleration $\ddot{\theta}$:

$$F_{s,sta} = \left[\left(F_{s,sta}\right)_0\right] + \left[\frac{\partial F_{s,sta}}{\partial n}\right] n + \frac{\partial F_{s,sta}}{\partial \dot{\theta}} \dot{\theta} + \frac{\partial F_{s,sta}}{\partial \ddot{\theta}} \ddot{\theta} \qquad (1a)$$

$$M_{b,sta} = \left[\left(M_{b,sta}\right)_0\right] + \left[\frac{\partial M_{b,sta}}{\partial n}\right] n + \frac{\partial M_{b,sta}}{\partial \dot{\theta}} \dot{\theta} + \frac{\partial M_{b,sta}}{\partial \ddot{\theta}} \ddot{\theta} \qquad (1b)$$

$$T_{sta} = \left[\left(T_{sta}\right)_0\right] + \left[\frac{\partial T_{sta}}{\partial n}\right] n + \frac{\partial T_{sta}}{\partial \dot{\theta}} \dot{\theta} + \frac{\partial T_{sta}}{\partial \ddot{\theta}} \ddot{\theta} \qquad (1c)$$

The quantities enclosed by brackets in equations (1) are, in the order of appearance, the basic and additional components of aerodynamic load. Equations (1a) to (1c) were solved by least-squares procedures by using the measured values of n, $\dot{\theta}$, $\ddot{\theta}$, and so forth, to obtain the bracketed quantities for each strain-gage station and each run. The components of loading caused by $\dot{\theta}$ and $\ddot{\theta}$ were found to be negligible for the runs analyzed, and these results are not presented in this report.

(When the dynamic pressure and Mach number are variable, the coefficients of n, $\dot{\theta}$, and $\ddot{\theta}$ and the intercepts $\left(F_{s,sta}\right)_0$, $\left(M_{b,sta}\right)_0$, and $\left(T_{sta}\right)_0$ are not constants. Since each of the runs analyzed contained some changes in q and M, a trial analysis of one run was made by the method described in appendix A to determine whether changes in q and M during a run should be taken into account. Equations (1a), (1b), and (1c) were found to be sufficiently accurate to determine values of the coefficients and intercepts corresponding to the average q and M of each run.)

In addition to the shears obtained from the wing strain-gage measurements, the total lift of the wing-fuselage-nacelles combination was determined from the known airplane weight W, the airplane normal load factor n, and the measured tail load L_T. The total load for the wing-fuselage-nacelles combination is simply $nW - L_T$. The aerodynamic shear at the airplane center line is one-half the total normal load. The time history of the center-line shear for the wing-fuselage-nacelles combination was separated into basic and additional components by the method

used for shears at other stations, expressed by the following equation, which is similar to equation (1):

$$\frac{1}{2}\left(nW - L_T\right) = \frac{1}{2}\left(nW - L_T\right)_0 + \frac{1}{2}\frac{\partial\left(nW - L_T\right)}{\partial n} n + \frac{1}{2}\frac{\partial\left(nW - L_T\right)}{\partial \dot{\theta}} \dot{\theta} + \frac{1}{2}\frac{\partial\left(nW - L_T\right)}{\partial \ddot{\theta}} \ddot{\theta} \tag{2}$$

or

$$F_{s,cl} = -\frac{1}{2} L_{T_0} + \frac{\partial F_{s,cl}}{\partial n} n + \frac{1}{2}\frac{\partial\left(nW - L_T\right)}{\partial \dot{\theta}} \dot{\theta} + \frac{1}{2}\frac{\partial\left(nW - L_T\right)}{\partial \ddot{\theta}} \ddot{\theta} \tag{2a}$$

The term $\frac{\partial F_{s,cl}}{\partial n}$ represents the additional component of aerodynamic shear at the airplane center line due to the lift of the wing-fuselage-nacelles combination. The additional aerodynamic shears, bending moments, and torques at each of the strain-gage stations, when divided by $\frac{\partial F_{s,cl}}{\partial n}$ produce the quantities

$$\text{Shear ratio} = \left(\frac{F_{s,sta}}{F_{s,cl}}\right)_{add}$$

$$M_b \text{ ratio} = \left(\frac{M_{b,sta}}{F_{s,cl}}\right)_{add}$$

$$\text{Torque ratio} = \left(\frac{T_{sta}}{F_{s,cl}}\right)_{add}$$

The quantities are the ordinates for the plots of figure 4. Parts (a), (b), and (c) of figure 4 give, respectively, the shear, bending moment, and torque at each strain-gage station per unit of additional aerodynamic shear at the center line of the wing-fuselage-nacelles combination. The curves in these plots represent the predictions of these quantities made by the method outlined in appendix B.

Because the theoretical calculations were made in terms of the parameter qm_R, it was considered appropriate to plot both predicted

and experimental results against qm_R for purposes of comparison and evaluation. Therefore, the abscissas for the experimental ordinates in figures 4 and 5 are the values of the product of the average dynamic pressure q and the lift-curve slope m_R for the rigid airplane without the tail corresponding to the average Mach number of each run. The values of m_R were obtained from the curve of m_R against M derived from wind-tunnel tests and given in reference 6.

Additional-Load Centers of Pressure and Deflections

Spanwise and streamwise distances from the strain-gage reference stations to the centers of pressure of the additional airload outboard of each station were obtained from the data by dividing additional-airload bending-moment and torque ratios by the corresponding shear ratios. Thus,

$$y'_{sta} = \left(\frac{M_{b,sta}}{F_{s,sta}}\right)_{add} = \frac{\left(\frac{M_{b,sta}}{F_{s,cl}}\right)_{add}}{\left(\frac{F_{s,sta}}{F_{s,cl}}\right)_{add}}$$

$$x'_{sta} = \left(\frac{T_{sta}}{F_{s,sta}}\right)_{add} = \frac{\left(\frac{T_{sta}}{F_{s,cl}}\right)_{add}}{\left(\frac{F_{s,sta}}{F_{s,cl}}\right)_{add}}$$

The coordinates y'_{sta} and x'_{sta} are plotted against qm_R in figure 5. The predicted center-of-pressure coordinates obtained as described in appendix B are represented by the curves in figure 5.

Figure 6 shows the locations of the centers of pressure of the additional airload outboard of the 7.8-percent-semispan station, as they appear on a plan-form view of the wing. Further use was made of the additional aerodynamic shears obtained by the use of equations (1a) and (2a) in order to calculate wing deflections due to additional airload. These calculations were made for only one run for the purpose of comparison with some of the results of deflection measurements reported in reference 2. Run 16 (table II) was found to be nearly equivalent to a maneuver (flight 4, run 20) of reference 2 except for a slight difference in gross airplane weight. The additional shears at each station obtained from the analysis of run 16 were adjusted for this weight difference.

Deflections at each of eight optigraph target stations were calculated from these adjusted shears by the use of an influence-coefficient matrix derived from the experimental data reported in reference 7. This matrix gives the optigraph target deflections due to concentrated loads applied at each of nine stations along the wing quarter-chord locus. The wing was divided into nine segments, each with one of the loading stations at its midpoint. The change in shear over any one segment was considered to be a load concentrated at the midpoint of the segment. These changes in shear were estimated by plotting the adjusted shears from run 16 against span station, fairing a curve through these points, and reading the shears at the segment boundaries. The average results of right and left wings were used at the 7.8-percent-semispan station.

The deflections thus calculated are those due to additional airload only, while those measured in flight include the deflections due to inertia load. The deflections due to inertia load are given in reference 2. These were subtracted from the deflections given for run 20 in order to obtain deflections due to additional airload.

The deflections calculated from the measured loads are compared with the results of deflection measurements in figure 7, where both sets of deflections are plotted against span station. The missing points in the measured deflections are the result of failure of two of the optigraph lights.

Basic Loadings

The intercepts of the measured aerodynamic loadings at zero load factor, the first term in equations (1), do not necessarily represent the true basic shears, bending moments, and torques. This fact is illustrated in figure 8, which shows the left-wing root-shear intercepts at zero load factor plotted against qm_R for the different altitudes of the test maneuvers. A curve faired through the points at any single altitude would be expected to pass through the origin of the plot because there can be no aerodynamic load if qm_R is zero. Obviously, this condition is not met in figure 8; rather, the points at each altitude appear to lie on a nearly straight line, the line for one altitude being approximately parallel to the lines for the other altitudes. Similar plots of the other basic load quantities showed the same kind of zero shifts.

An equation representing all the basic shears at one station by a function of qm_R, while allowing a different intercept for each altitude, is as follows:

$$\left(F_{s,sta}\right)_0 = A\left(qm_R\right) + B\left(qm_R\right)^2 + \Delta F_{s,30} + \Delta F_{s,25} + \Delta F_{s,20} + \Delta F_{s,15} \quad (3)$$

The ΔF_s terms in equation (3) are considered to be the zero shifts in the measured load with changes in altitude, and the numerical subscript indicates the altitude (in thousands of feet) to which each pertains.

Values of ΔF_s obtained by least-squares procedures were applied as corrections to the basic shears. Similar corrections were made to the basic bending moments and torques.

The resulting adjusted basic loads are presented in figure 9. Parts (a), (b), and (c) of figure 9 show, respectively, the basic shears, bending moments, and torques from equations (1) adjusted by the method described by equation 3 for each strain-gage station and each run. The abscissas are again the average values of qm_R for each run. The basic shears, bending moments, and torques predicted by the method outlined in appendix B are given by the curves in figure 9.

DISCUSSION

Additional-Load Quantities

The curves of figure 4 show that the predicted additional aerodynamic loading quantities agree well with those determined from flight-test measurements. In each case, the experimental results form a curve which is approximately parallel to the predicted curve, though in some cases there are noticeable differences in level. These differences in level may be due to slight errors in either the flight measurements or the wind-tunnel measurements on which the predictions were based. The possibility of small measuring errors is indicated by the consistent differences between the measurements at 7.8 percent semispan on the right and left wings, especially in figure 4(a); however, because the measured right and left shear ratios are both below the predicted curve, it is possible that the wing outboard of the fuselage carried somewhat less than the predicted fraction of the total load. From the wind-tunnel pressure-distribution tests, the exact fraction of load carried by the fuselage was indeterminate. The load-distribution curve from that source was, therefore, faired smoothly into the center line to obtain the predicted results at zero qm_R.

Small discrepancies in level at zero qm_R apparently have little effect on the predicted changes in the additional-load shear, bending moment, and torque ratios, because the predicted results approximately parallel the experimental results, even at the highest values of qm_R.

The small scatter in the flight results is apparently random. No correlation could be found between changes in airplane weight and the displacement of the points from an average curve. This result was to be expected because of the relatively small changes in airplane weight.

The quantities given in figure 4 are considered to be primary quantities. From these quantities the center-of-pressure coordinates in figure 5 were obtained. The discrepancies in figure 5 between predicted and experimental results are associated with discrepancies previously noted in connection with figure 4. The greatest of these discrepancies are at 7.8 percent semispan, where there are large differences between experimental results for right and left wings and at the 36.2-percent station. All major differences between predicted and experimental center-of-pressure coordinates are seen to be the result of relatively smaller differences in the quantities of figure 4.

The center-of-pressure results for the wing-root station may be taken as representative of the changes in additional-load center of pressure of the entire wing-body-nacelle configuration caused by flexibility. Figure 6 shows the locations of the centers of pressure of the additional airload outboard of the 7.8-percent-semispan stations, as they appear on a plan-form view of the wing. Only that section of the wing is shown which contains the centers of pressure and $M.A.C._1$, the mean aerodynamic chord of the area outboard of 7.8 percent of $b/2$. The quarter-chord locus is given also. Experimental results for both right and left wing have been plotted together for easy comparison, and the predicted results for the flight range of qm_R are given by the curve. The direction of movement is inboard and forward with increasing qm_R, as designated by the arrow. Because of the effect of the inboard engine nacelles, both experimental and theoretical centers of pressure lie on loci somewhat forward of the quarter-chord locus. Had the effects of the nacelles been neglected in predicting the loadings, the predicted centers of pressure would have fallen on the quarter-chord locus.

Although the initial location of the center of pressure (at the lowest value of qm_R) is in doubt because of the discrepancies between experiment and prediction and also between the two sets of experimental results in figure 6, it is fairly well established that the changes in additional-load center of pressure were accurately predicted and that the effects of nacelle loads are not negligible for this airplane. The fact that the nacelle effects were strong enough to give a center-of-pressure location noticeably forward of that which would be predicted for the wing alone indicates that the nacelles should also have an appreciable effect on the changes in center of pressure due to flexibility. For the change in center-of-pressure location with change in qm_R, theoretical calculations show that, over the qm_R range from 0 to

50, the movement of the center of pressure for the wing alone would be about 18 percent greater than that calculated for the wing plus nacelles. (A line representing the predicted center-of-pressure locus for the wing alone in figure 6 would fall on the wing quarter-chord locus and would be approximately 18 percent longer than the line shown.) The combined effects of the inboard nacelle are, therefore, to move the center-of-pressure locus forward of the wing quarter-chord line and to decrease the amount of center-of-pressure movement over a given qm_R range.

Correlation With Deflection Measurements

The comparison of wing deflections obtained directly from flight measurements with those calculated from measured loads shows a high degree of correlation between the two different types of flight-test measurements (fig. 7). Although it is not shown in figure 7, the substitution of predicted shears for measured shears in the deflection calculations yielded almost identical results. This agreement of results is an indication that the differences between experimental and predicted shear ratios in figure 4(a) are not significant where wing-deflection calculations are concerned.

Basic-Load Quantities

The agreement which was obtained between predicted and measured basic shears, bending moments, and torques in figure 9 is fairly good. It should be stated that strain gages are not entirely suited to the measurement of basic loads because of their response to strains produced by changes in temperature as well as to those produced by actual loads. The strain gages near the nacelles may be subject to the effects of changes in engine temperature, and these changes are nearly proportional to qm_R. These effects cannot be detected by the method of zero-shift correction described in the section entitled "Method and Results"; furthermore, the theoretical calculation of basic loads is dependent upon a number of wind-tunnel measurements of relatively small pitching-moment coefficients. Errors in the wind-tunnel measurements of wing and nacelle pitching moments would cause relatively larger errors at the outboard stations than at the root station. The root-station basic loads are mainly affected by the zero-lift pitching-moment coefficient for the entire airplane without the tail.

The maximum basic shears occurring at the root station are about 7 percent of the maximum structural shear for which that station was designed. While the basic loads are not negligible from the structual design standpoint, an error as great as 20 percent in their determination could probably be tolerated. The actual discrepancies between

predicted and experimental root-station basic loadings are much less than this.

The greatest differences, percentagewise, occur at the two stations near the engine nacelles. This might be expected from the previous statements about strain-gage response to temperature gradients and the dependence of the calculated loads at the outboard stations on the measurement of relatively small quantities by wind-tunnel testing.

CONCLUSIONS

Aerodynamic shears, bending moments, and torques measured on the wing of a B-47A airplane during quasi-static symmetrical maneuvers have been analyzed in order to obtain basic and additional components. The values of these components were then compared with values of the same quantities predicted by the theoretical extension of low-speed wind-tunnel measurements. As a result of the analysis and comparison, the following conclusions are drawn:

1. Additional-load quantities, including centers of pressure, can be adequately predicted. Changes in these quantities with increasing values of the parameter qm_R can be accurately determined by the theoretical methods available.

2. Basic shears, bending moments, and torques can be adequately predicted, especially near the root.

3. A comparison of deflections calculated from measured loads with deflections measured in flight shows good correlation between the two different types of measurements. Both sets of experimental deflections agree well with theoretical deflections.

Langley Aeronautical Laboratory,
National Advisory Committee for Aeronautics,
Langley Field, Va., May 9, 1957.

APPENDIX A

EFFECTS OF CHANGING DYNAMIC PRESSURE AND MACH NUMBER ON ANALYSIS

In order to determine the effect on the coefficients of changes in dynamic pressure and Mach number during a run, a single maneuver was analyzed by two methods. One of the methods was based on the assumption that the additional- and basic-load quantities for the average dynamic pressure and Mach number of a run would be obtained if changes in q and M within the run were neglected. The other method assumed linear variations of basic and additional quantities with changes in the parameter qm_R. The deviations from the average value of qm_R were used to establish the average basic and additional quantities for the run. Run 26 was used for this purpose. (See table II for variations in q and M.)

The bending moment at the root station was considered to be most likely to show the effects of q and M changes. For the first method used, the equation for bending moment in terms of load factor n, pitching velocity $\dot{\theta}$, and pitching acceleration $\ddot{\theta}$ was written as

$$M_{b,sta} = \left[\left(M_{b,sta}\right)_0\right]_{av} + \left[\frac{\partial M_{b,sta}}{\partial n}\right]_{av} n + \frac{\partial M_{b,sta}}{\partial \dot{\theta}} \dot{\theta} + \frac{\partial M_{b,sta}}{\partial \ddot{\theta}} \ddot{\theta} \qquad (A1)$$

The terms in brackets are of primary interest. $\left[\left(M_{b,sta}\right)_0\right]_{av}$ is the basic bending moment when all other quantities are zero, and $\left[\frac{\partial M_{b,sta}}{\partial n}\right]_{av}$ is the additional aerodynamic bending moment.

Because both bracketed quantities in equation (A1) would be expected to vary with q and M as the product of q and the lift-curve slope m_R of the rigid airplane without the tail, the corresponding equation for the second method was written as

$$\left(M_{b,sta}\right)_0 = \left[\left(M_{b,sta}\right)_0\right]_{av} + K_0 \Delta\left(qm_R\right) \qquad (A2)$$

$$\frac{\partial M_{b,sta}}{\partial n} = \left(\frac{\partial M_{b,sta}}{\partial n}\right)_{av} + K_n \Delta\left(qm_R\right) \qquad (A3)$$

where

$$\Delta\left(qm_R\right) = qm_R - \left(qm_R\right)_{av}$$

The quantities K_0 and K_n are constants if a linear variation of $M_{b,0}$ and $\frac{\partial M_{b,sta}}{\partial n}$ with qm_R is assumed over the range of qm_R for a single run. Substituting equations (A2) and (A3) into (A1) gives

$$M_{b,sta} = \left[\left(M_{b,sta}\right)_0\right]_{av} + K_0\,\Delta\left(qm_R\right) + \left(\frac{\partial M_{b,sta}}{\partial n}\right)_{av} n + K_n\,\Delta\left(qm_R\right)n + \frac{\partial M_{b,sta}}{\partial \dot{\theta}}\,\dot{\theta} + \frac{\partial M_{b,sta}}{\partial \ddot{\theta}}\,\ddot{\theta} \tag{A4}$$

For the purposes of the analysis represented by equation (A4), the assumption that changes in m_R are given by the Glauert factor for swept wings is sufficiently accurate. If the lift-curve slope at zero Mach number is denoted by $\left(m_R\right)_{M=0}$, the lift-curve slope at any Mach number is

$$m_R = \frac{\left(m_R\right)_{M=0}}{\sqrt{1 - M^2\cos^2\Lambda}}$$

and

$$qm_R = \frac{\left(qm_R\right)_{M=0}}{\sqrt{1 - M^2\cos^2\Lambda}}$$

It is not necessary that m_{R_0} be known since it can be included in the unknown coefficient of $\Delta\left(qm_R\right)$ in equation (A4). The quantity $\left(m_R\right)_{M=0}\,\Delta\,\frac{q}{\sqrt{1 - M^2\cos^2\Lambda}}$ is substituted for $\Delta\left(qm_R\right)$ and gives

$$M_{b,sta} = \left[\left(M_{b,sta}\right)_0\right]_{av} + K_0\left(m_R\right)_{M=0} \Delta \frac{q}{\sqrt{1 - M^2\cos^2\Lambda}} + \left[\frac{\partial M_{b,sta}}{\partial n}\right]_{av} n +$$

$$K_n\left(m_R\right)_{M=0} \Delta \frac{q}{\sqrt{1 - M^2\cos^2\Lambda}} n + \frac{\partial M_{b,sta}}{\partial \dot{\theta}} \dot{\theta} + \frac{\partial M_{b,sta}}{\partial \ddot{\theta}} \ddot{\theta} \qquad (A5)$$

Equations (A1) and (A5) were each solved by least-squares methods by using 25 points from the time histories of bending moment, load factor, q, M, $\dot{\theta}$, and $\ddot{\theta}$ for run 26. The basic and additional components of bending moment from each equation and the probable errors of fit are given in the following table for comparison:

Equation	$\frac{\partial M_{b,sta}}{\partial n}$, in-lb/g	$\left[\left(M_{b,sta}\right)_0\right]_{av}$, in-lb	Probable error, in-lb
(A1)	12.16×10^6	0.13×10^6	0.065×10^6
(A5)	12.21×10^6	$.12 \times 10^6$	$.065 \times 10^6$

Because the results from equation (A1) are nearly the same as those from equation (A5), the basic and additional-load components corresponding to the average qm_R of any run of these tests could be determined accurately, and with a considerable saving in time, by neglecting changes in q and M during a run.

The coefficients for $\dot{\theta}$ and $\ddot{\theta}$ were indeterminate because of the very small changes in these quantities.

APPENDIX B

THEORETICAL ADDITIONAL AND BASIC LOADS

The additional aerodynamic wing-load distribution was calculated by considering separately the effects of angle-of-attack and load-factor changes. The matrix method given in reference 8 was used in combination with the superposition method of solution given in reference 9. This method of solution was modified to incorporate least-squares methods of curve fitting in order to define the elastic twist distributions in terms of span station.

The required aerodynamic and structural influence-coefficient matrices were calculated for nine stations along the semispan. The spanwise distribution of section-lift-curve slopes for the rigid wing was determined from low-speed wind-tunnel pressure-distribution tests (ref. 10) by the method of reference 8.

The equilibrium load distributions resulting from a unit symmetrical change in wing root angle of attack were computed for a number of values of the product of the dynamic pressure q and the lift-curve slope m_R of the rigid airplane without the tail while the load factor was held constant. Since both fuselage overvelocity effects and nacelle lift and pitching-moment effects are proportional to angle of attack (see ref. 8), these effects were superposed on the uniform unit angle of attack. Overvelocity effects were estimated from the equations in reference 8, and the nacelle lift and pitching moment were estimated from wind-tunnel tests. Values of qm_R were chosen which would approximately cover the range of the flight tests and which would permit defining a smooth curve.

The equilibrium airload distributions due to wing inertia twist per unit airplane load factor were similarly calculated while the root angle of attack was held constant.

The results of the two preceding steps were, for each value of qm_R, the partial derivative of aerodynamic load with respect to root angle of attack and the partial derivative of aerodynamic load with respect to load factor, for each of the nine span stations. Successive integrations of these load distributions gave the partial derivatives of shear and bending moment with respect to angle of attack and load factor. Torques were obtained by integration along the streamwise projection of the wing quarter-chord locus. Concentrated nacelle loads were added at the proper stations in each case.

The derivative of the aerodynamic shear, bending moment, or torque at a particular wing station with respect to airplane normal-load factor is related to the partial derivatives of the particular loading with respect to angle of attack and load factor and to the total derivative of root angle of attack with respect to load factor. The following equation, which applies to shear, is an example of this relationship.

$$\frac{dF_{s,sta}}{dn} = \frac{\partial F_{s,sta}}{\partial \alpha_r} \frac{d\alpha_r}{dn} + \left(\frac{\partial F_{s,sta}}{\partial n}\right)_{inertia} \tag{B1}$$

The term $\left(\frac{\partial F_{s,sta}}{\partial n}\right)_{inertia}$ in equation (B1) is the airload caused by wing twisting due to inertia load and must not be confused with the inertia load itself.

At the airplane center line, the derivative of shear with respect to load factor is known to be $\frac{1}{2}\left(W - \frac{dL_T}{dn}\right)$. At the center line, therefore,

$$\frac{1}{2}\left(W - \frac{dL_T}{dn}\right) = \frac{\partial F_{s,cl}}{\partial \alpha_r} \frac{d\alpha_r}{dn} + \left(\frac{\partial F_{s,cl}}{\partial n}\right)_{inertia} \tag{B2}$$

Equation (B2) was used to determine $\frac{d\alpha_r}{dn}$ for each value of qm_R for which values of the partial derivatives were calculated and for several values of $W - \frac{dL_T}{dn}$ which covered the range of the flight-test values. The values of $\frac{d\alpha_r}{dn}$ thus calculated were inserted in equation (B1) in order to obtain the additional shear, bending moment, and torque at each station for each value of qm_R and for each value of $W - \frac{dL_T}{dn}$. These shears, bending moments, and torques were nondimensionalized with respect to the additional center-line shear $\frac{1}{2}\left(W - \frac{dL_T}{dn}\right)$, just as were the experimental results. The changes in these loading ratios caused by changes in $W - \frac{dL_T}{dn}$ were found to be negligible, even for a 20-percent change in $W - \frac{dL_T}{dn}$. The theoretical loading ratios corresponding

to $W - \frac{dL_T}{dn} = 110{,}000$, approximately the average flight-test value, were used for comparison with the flight-test results.

The predicted additional-load shear, bending-moment, and torque ratios were plotted against qm_R and appear in figure 4 in comparison with the flight-test results.

At zero load factor for the airplane, the sum of the normal airloads on the airplane must be zero. Simultaneously, the sum of the pitching moments about any pitch axis must also be zero.

At the airplane center line, the shears due to the aerodynamic forces on one-half of the airplane at zero load factor are:

1. Wing shear due to root angle of attack, $\frac{\partial F_{s,cl}}{\partial \alpha_r}$

2. Wing shear due to twisting of the wing by wing and nacelle aerodynamic pitching moments, $\left(F_{s,t}\right)_{cl}$

3. Wing shear due to fuselage overvelocity, described in reference 8, $\left(F_{s,over}\right)_{cl}$

4. Horizontal-tail aerodynamic load, $\frac{1}{2} L_{T,0}$

5. Nacelle airload, $\left(F_{s,nac}\right)_{cl}$

Equating the sum of the vertical forces to zero gives the following equation:

$$\frac{\partial F_{s,cl}}{\partial \alpha_r}\left(\alpha_r - \alpha_0\right) + \left(F_{s,t}\right)_{cl} + \left(F_{s,over}\right)_{cl} + \left(F_{s,nac}\right)_{cl} + \frac{L_{T,0}}{2} = 0 \tag{B3}$$

Each of the forces in equation (B3) may exert a pitching moment about an axis through the quarter-chord point of the mean aerodynamic chord. In addition, there will be a pitching moment about this axis due to the aerodynamic pitching-moment coefficient $C_{M,0}$ of the airplane without the tail. Equating the sum of the pitching moments to zero gives:

$$\frac{\partial F_{s,cl}}{\partial \alpha_r}\left(\alpha_r - \alpha_0\right)\Delta x'_{\alpha_r} + \left(F_{s,t}\right)_{cl}\Delta x'_t + \frac{L_{T,0}}{2}\Delta x'_T + C_{M,0}qS\frac{\bar{c}}{2} = 0 \qquad (B4)$$

where $\Delta x'$ is the distance measured from 0.25 mean aerodynamic chord streamwise to the center of pressure of the load indicated in the subscript.

In order to compute the components of equations (B3) and (B4), the pitching-moment coefficients of the wing, nacelles, and airplane without the tail were estimated from the wind-tunnel-test results given in reference 6. Each of these coefficients was assumed to vary with Mach number as m_R does.

Using the aerodynamic and structural influence-coefficient matrices and methods of solution which were used in the additional-load calculations, distributions of $F_{s,t}$, $\frac{\partial F_s}{\partial \alpha_r}$, and $F_{s,over}$ were calculated for each of a number of values of qm_R. Bending-moment and torque distributions and the necessary $\Delta x'$ distances were also calculated. The pitching moments due to fuselage overvelocity and engine nacelles do not appear in equation (B4). These quantities are included in the $C_{M,0}$ term as measured in the wind-tunnel tests.

In both equations (B3) and (B4), only $L_{T,0}$ and $\alpha_r - \alpha_0$ are unknown. These quantities were obtained by simultaneous solution of equations (B3) and (B4) for each value of qm_R.

At any strain-gage station, the basic shear is

$$\left(F_{s,0}\right)_{sta} = \left(F_{s,t}\right)_{sta} + \frac{\partial F_{s,sta}}{\partial \alpha_r}\left(\alpha_r - \alpha_0\right) + \left(F_{s,over}\right)_{sta} + \left(F_{s,nac}\right)_{sta} \qquad (B5)$$

All quantities on the right-hand side of equation (B5) are known as a result of the preceding computations.

The bending moment and torque due to load were computed from their component parts by equations similar to equation (B5). The torque due to load was added to the torque due to wing and nacelle aerodynamic pitching moments in order to obtain the basic torque for each station and each value of qm_R.

REFERENCES

1. Aiken, William S., Jr., and Fisher, Raymond A.: Lift-Curve Slope Determined in Flight on a Flexible Swept-Wing Jet Bomber. NACA RM L56E21a, 1956.

2. Mayo, Alton P., and Ward, John F.: Flight Investigation and Analysis of the Wing Deformations of a Swept-Wing Bomber During Push-Pull Maneuvers. NACA RM L54K24a, 1955.

3. Mayo, Alton P., and Ward, John F.: Flight Investigation and Analysis of the Wing Deformations on a Swept-Wing Bomber During Rolling Maneuvers. NACA RM L56C23a, 1956.

4. Cooney, T. V., Andrews, William H., and McGowan, William A.: Preliminary Results From Flight Measurements in Gradual-Turn Maneuvers of the Wing Loads and the Distribution of Load Among the Components of a Boeing B-47A Airplane. NACA RM L55B02, 1955.

5. Skopinski, T. H., Aiken, William S., Jr., and Huston, Wilber B.: Calibration of Strain-Gage Installations in Aircraft Structures for the Measurement of Flight Loads. NACA Rep. 1178, 1954. (Supersedes NACA TN 2993.)

6. Gray, E. Z., Sandoz, P., and Entz, H.: Design Load Criteria. [Model B-47B.] Vol. I. Document No. D-9441 (Contract No. W33-038 ac-22413), Boeing Airplane Co., Nov. 9, 1948.

7. Mayo, Alton P., and Ward, John F.: Experimental Influence Coefficients for the Deflection of the Wing of a Full-Scale, Swept-Wing Bomber. NACA RM L53L23, 1954.

8. Gray, W. L., and Schenk, K. M.: A Method for Calculating the Subsonic Steady-State Loading on an Airplane With a Wing of Arbitrary Plan Form and Stiffness. NACA TN 3030, 1953.

9. Brown, R. B., Holtby, K. F., and Martin, H. C.: A Superposition Method for Calculating the Aeroelastic Behavior of Swept Wings. Jour. Aero. Sci., vol. 18, no. 8, Aug. 1951, pp. 531-542.

10. Spangler, T. A.: The Span-Load Distribution of the XB-47 Wing. Document No. D-8055, Boeing Airplane Co., Dec. 24, 1946.

TABLE I

WING DIMENSIONS AND CHARACTERISTICS OF THE B-47A AIRPLANE

Span, ft	116.0
Area, sq ft	1,428.0
Aspect ratio	9.43
Taper ratio	0.42
Thickness ratio (constant)	0.12
Mean aerodynamic chord, in.	155.9
Sweep of 0.25-percent-chord line, deg	35.0
Root chord, in.	208.0
Tip chord, in.	87.0
Airfoil section	BAC 145
Incidence (root and tip), deg	2.75
Dihedral, deg	0

TABLE II

FLIGHT CONDITIONS

[Center of gravity at 22.5 ± 1 percent mean aerodynamic chord for all runs]

Flight 25, run	Pressure altitude, ft	M_{av}	M_{max}	M_{min}	q_{av}, lb/sq ft	q_{max}, lb/sq ft	q_{min}, lb/sq ft	W, lb	$(qm_R)_{av}$
5	30,000	0.81	0.823	0.807	293	302	285	114,500	32.8
6	30,000	.76	.764	.760	258	259	255	114,200	27.9
7	30,000	.73	.745	.715	230	238	216	113,800	24.4
8	30,000	.67	.683	.654	197	206	187	113,400	20.1
9	30,000	.61	.626	.602	162	172	155	113,100	16.0
10	30,000	.56	.581	.545	141	151	131	112,700	13.5
11	25,000	.81	.817	.807	365	372	357	112,500	40.9
12	25,000	.77	.780	.755	335	349	318	112,200	36.4
13	25,000	.71	.715	.699	278	289	268	111,800	29.1
14	25,000	.66	.675	.647	244	259	230	111,300	24.8
15	25,000	.62	.645	.596	215	237	193	110,900	21.4
16	25,000	.57	.587	.544	178	196	161	110,600	17.2
17	20,000	.81	.818	.805	445	454	434	110,100	49.8
18	20,000	.76	.760	.750	387	398	379	109,800	41.8
19	20,000	.72	.780	.700	360	383	336	109,400	37.9
20	20,000	.66	.670	.655	294	311	278	109,100	29.9
21	20,000	.57	.592	.540	225	251	200	108,600	21.8
22	20,000	.47	.490	.428	145	168	123	107,700	13.4
23	15,000	.77	.773	.752	490	507	470	107,300	52.9
24	15,000	.71	.716	.692	425	445	408	107,000	44.4
25	15,000	.66	.669	.644	374	394	354	106,700	37.8
26	15,000	.56	.582	.542	270	294	247	105,900	26.1
27	15,000	.47	.494	.425	180	210	148	105,500	16.6

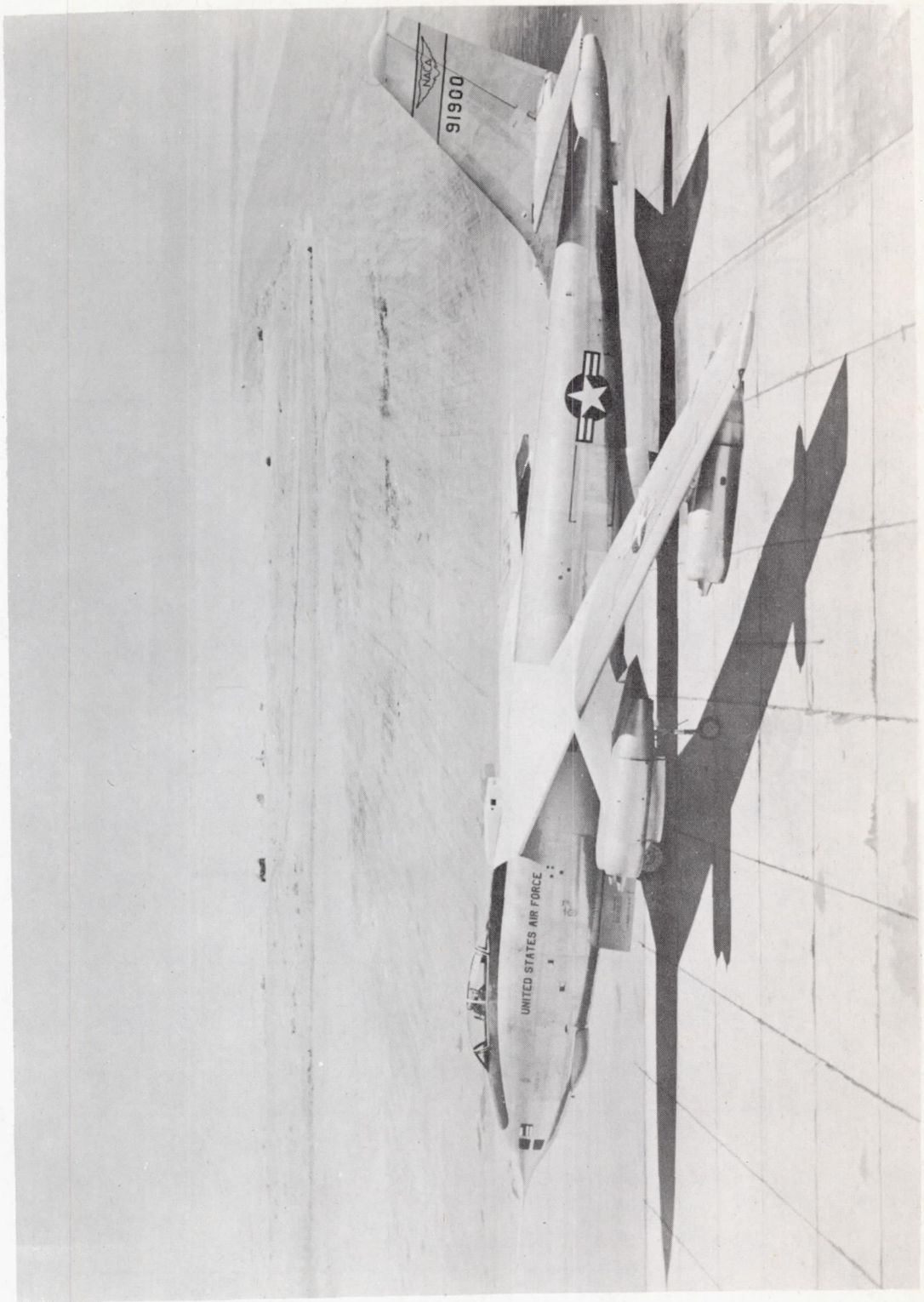

Figure 1.- Test airplane. L-86692

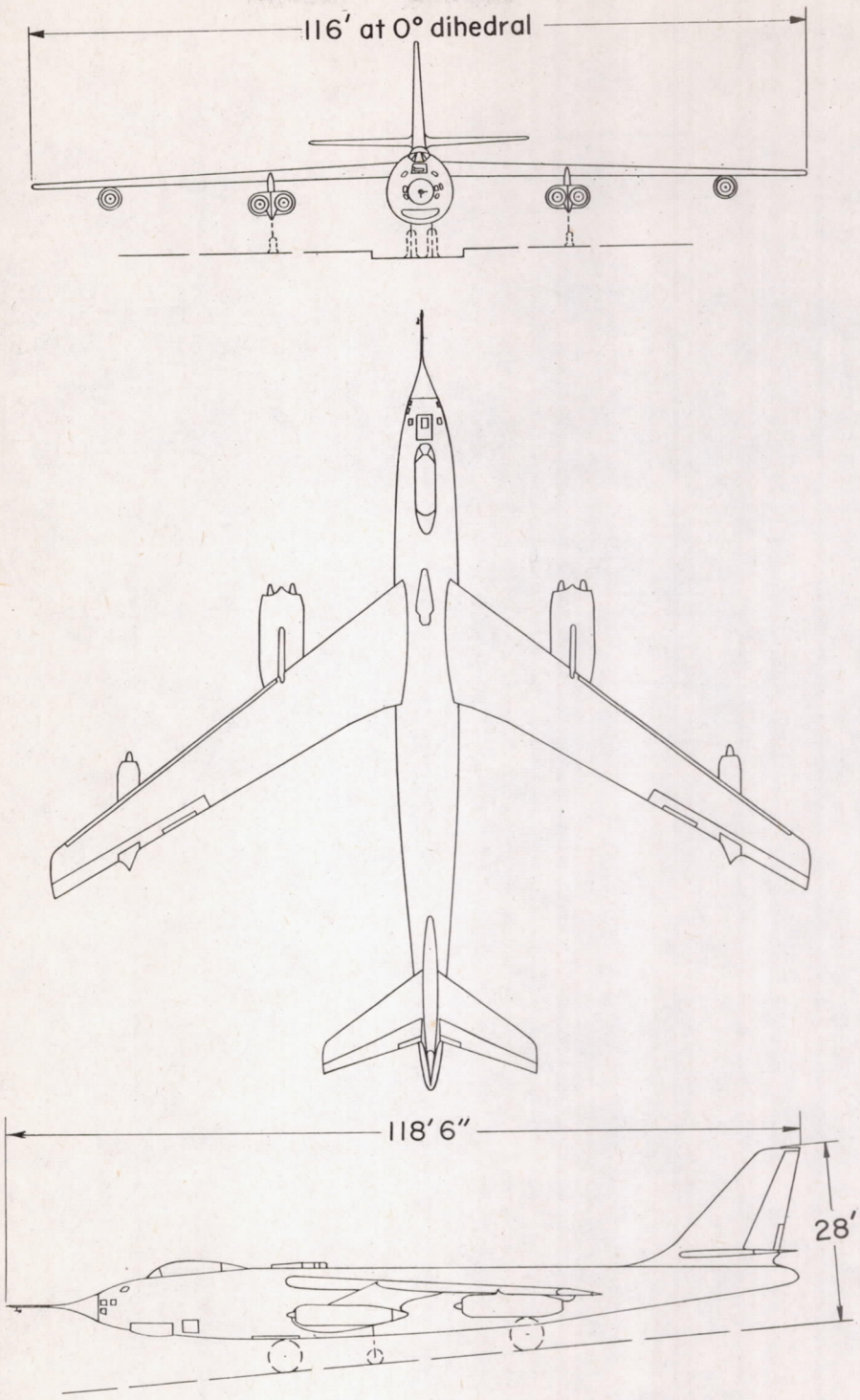

Figure 2.- Three views of test airplane.

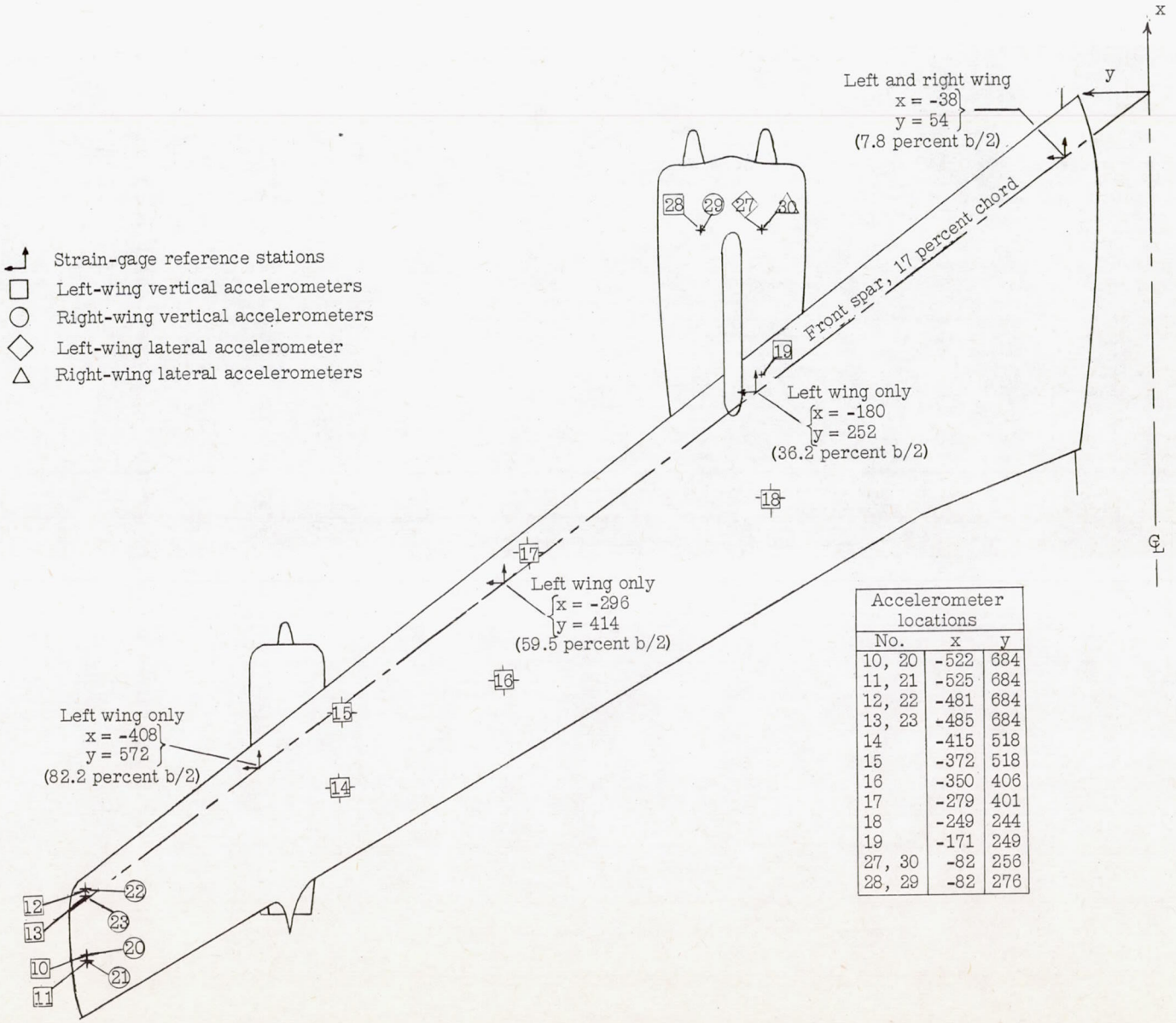

Accelerometer locations		
No.	x	y
10, 20	-522	684
11, 21	-525	684
12, 22	-481	684
13, 23	-485	684
14	-415	518
15	-372	518
16	-350	406
17	-279	401
18	-249	244
19	-171	249
27, 30	-82	256
28, 29	-82	276

Figure 3.- Strain-gage and accelerometer locations.

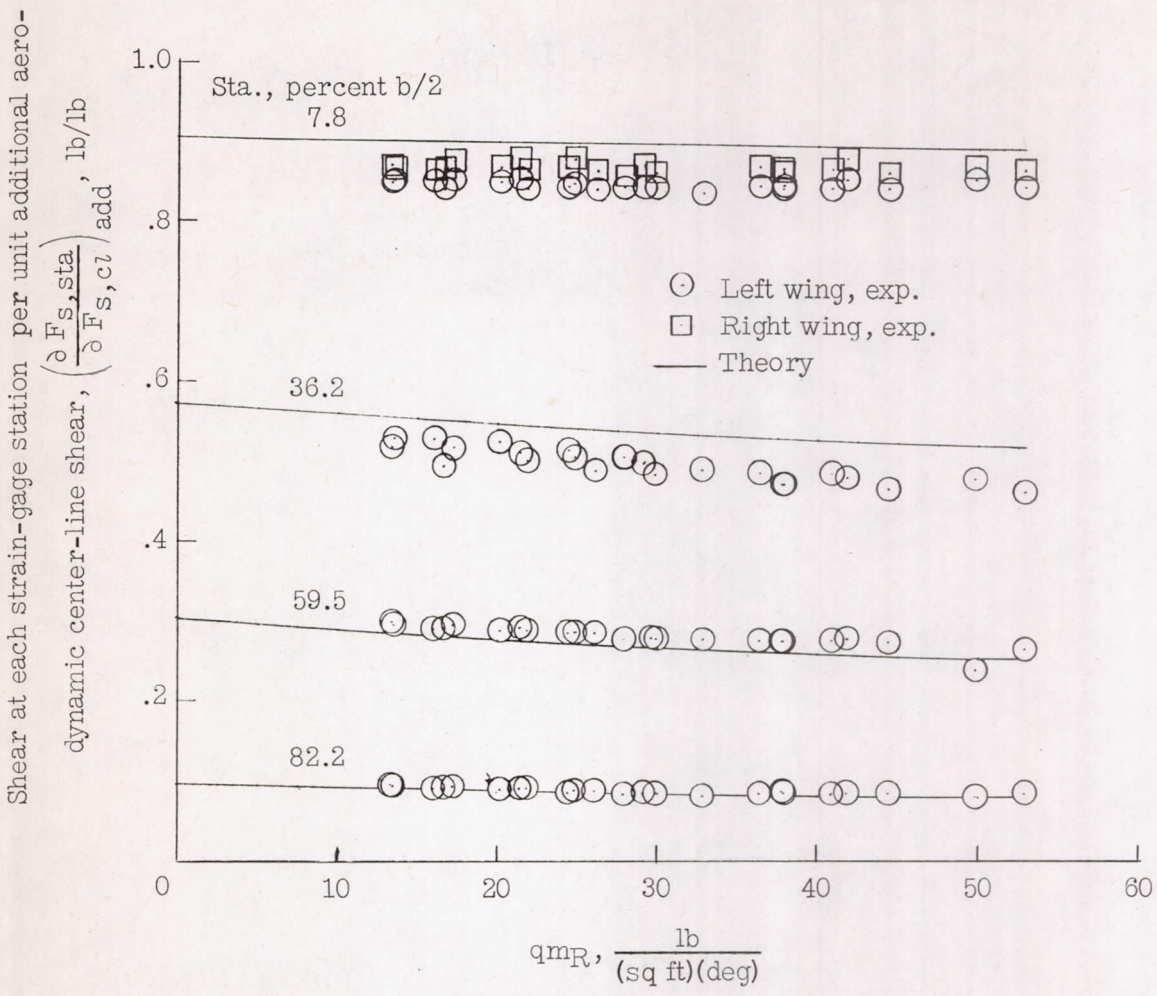

(a) Shear ratios.

Figure 4.- Comparison of experimental and predicted load ratios.

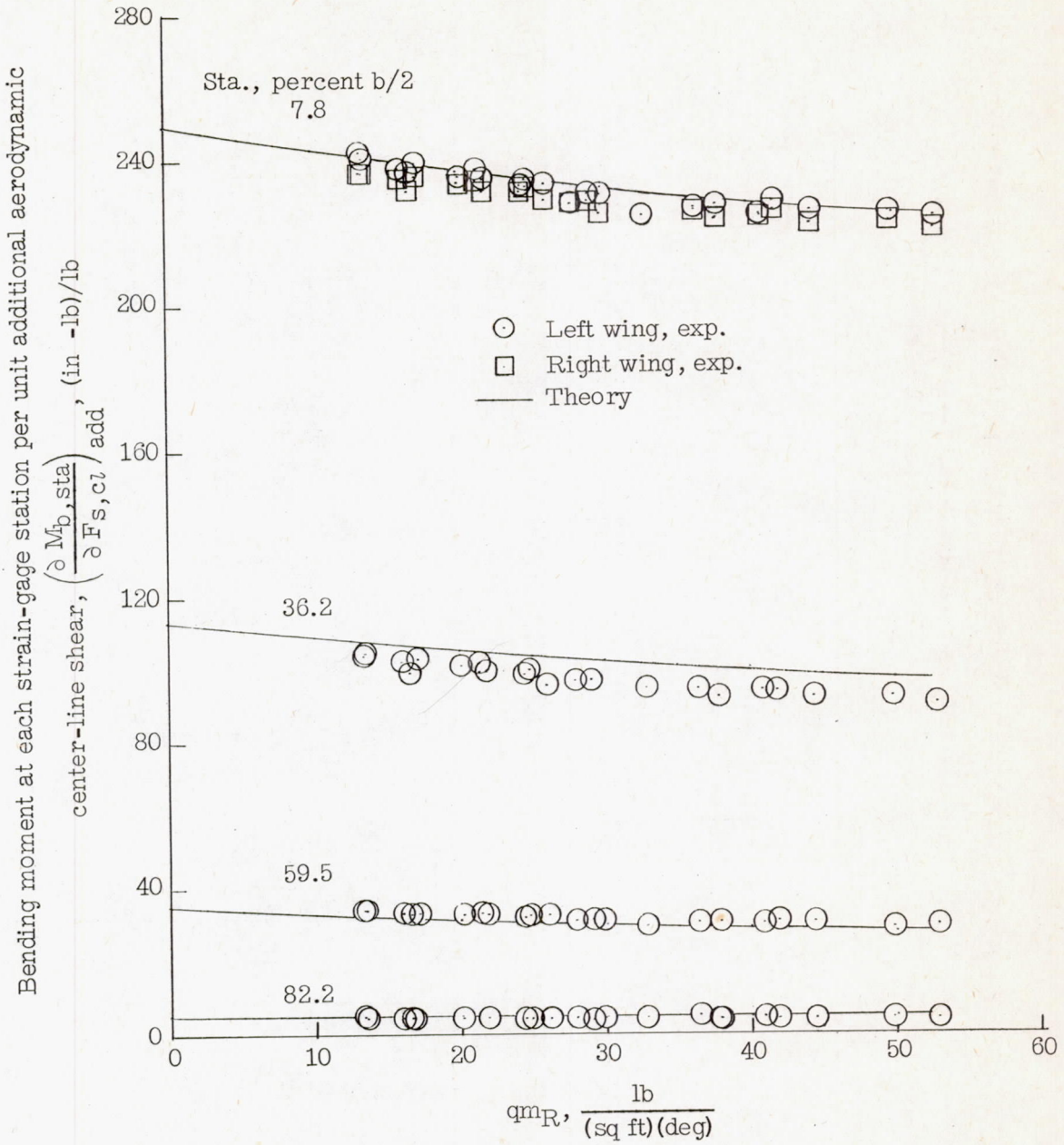

(b) Bending-moment ratios.

Figure 4.- Continued.

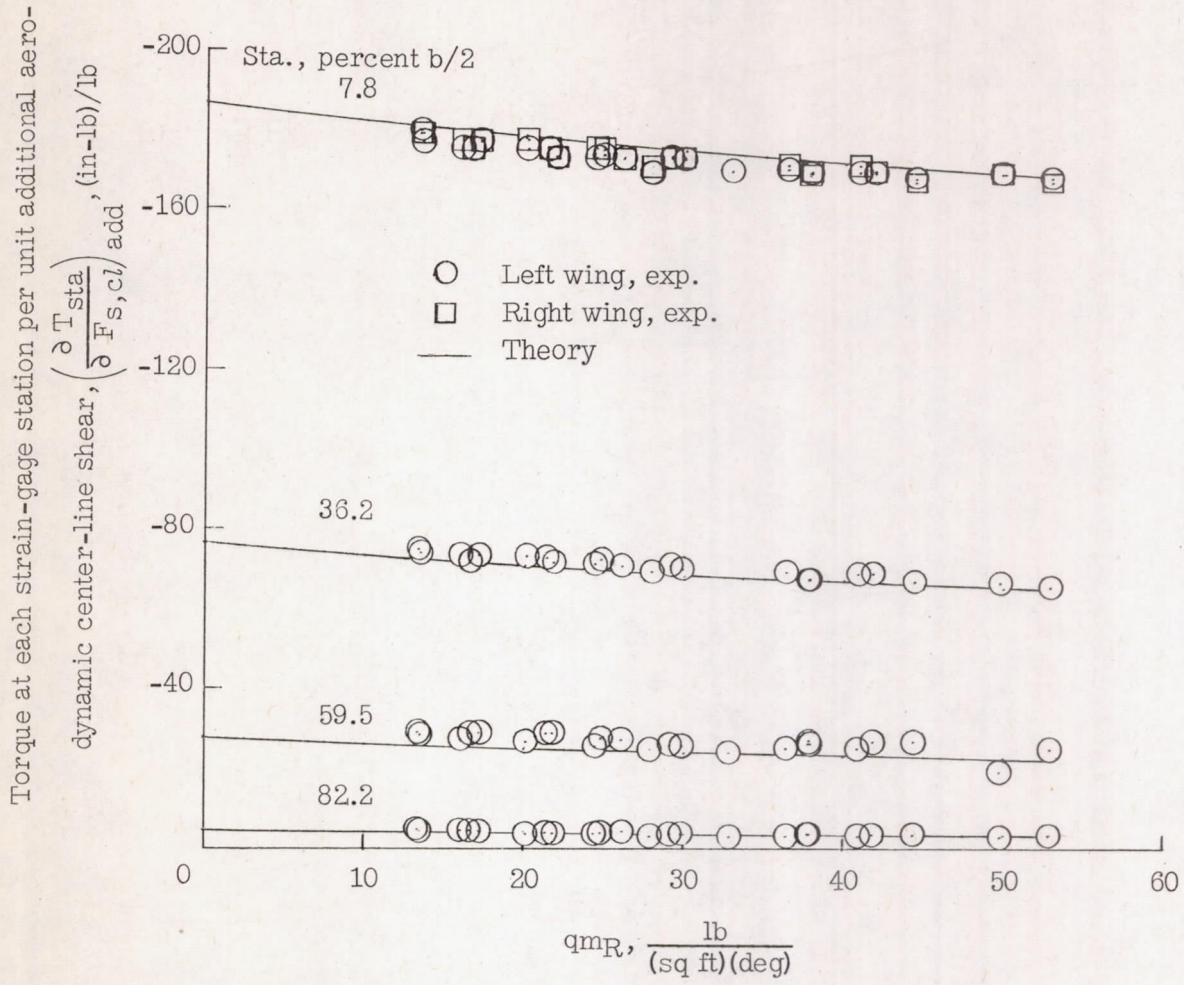

(c) Torque ratios.

Figure 4.- Concluded.

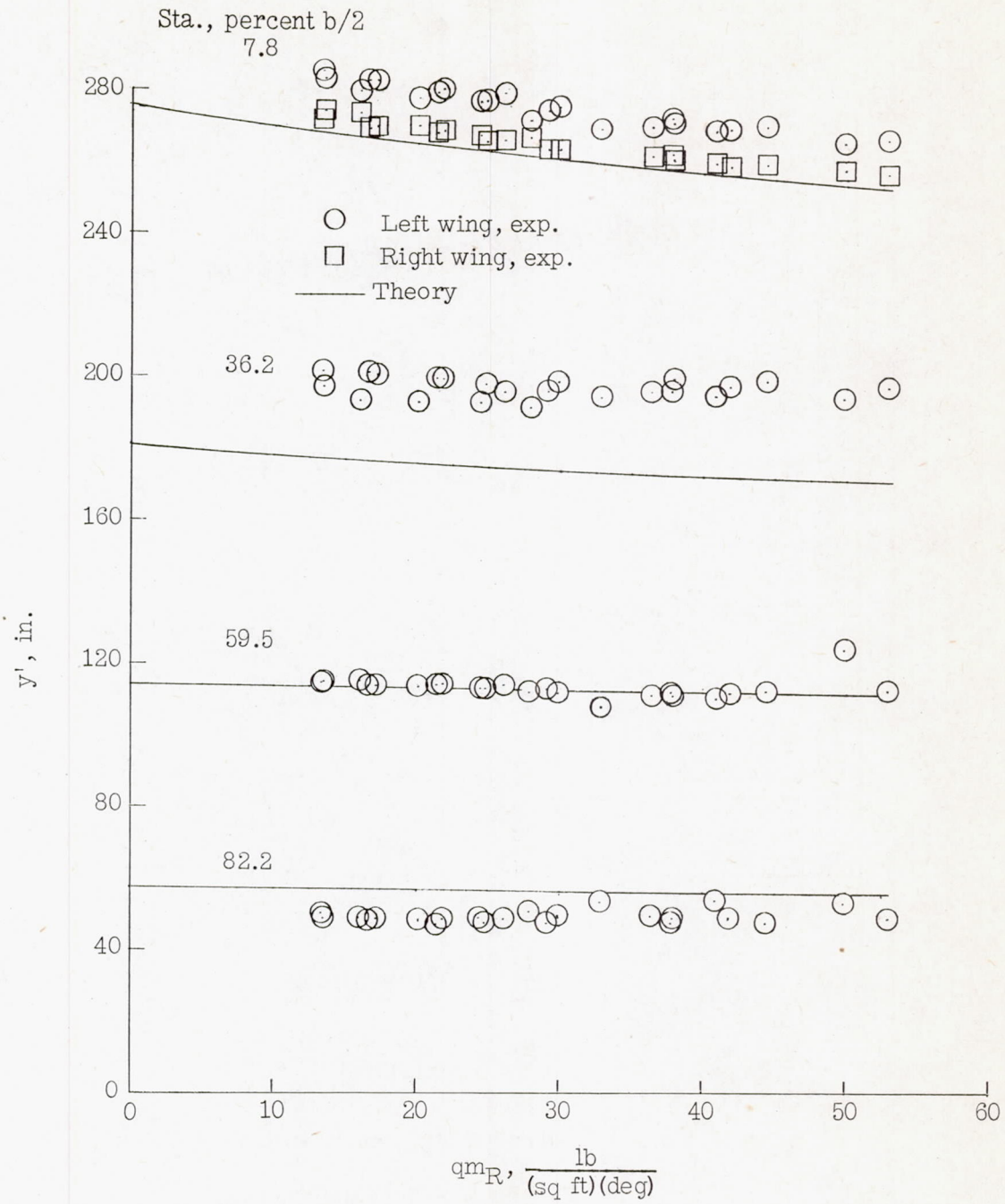

(a) Spanwise coordinates.

Figure 5.- Coordinates of centers of pressure of additional aerodynamic load against qm_R in comparison with predicted coordinates.

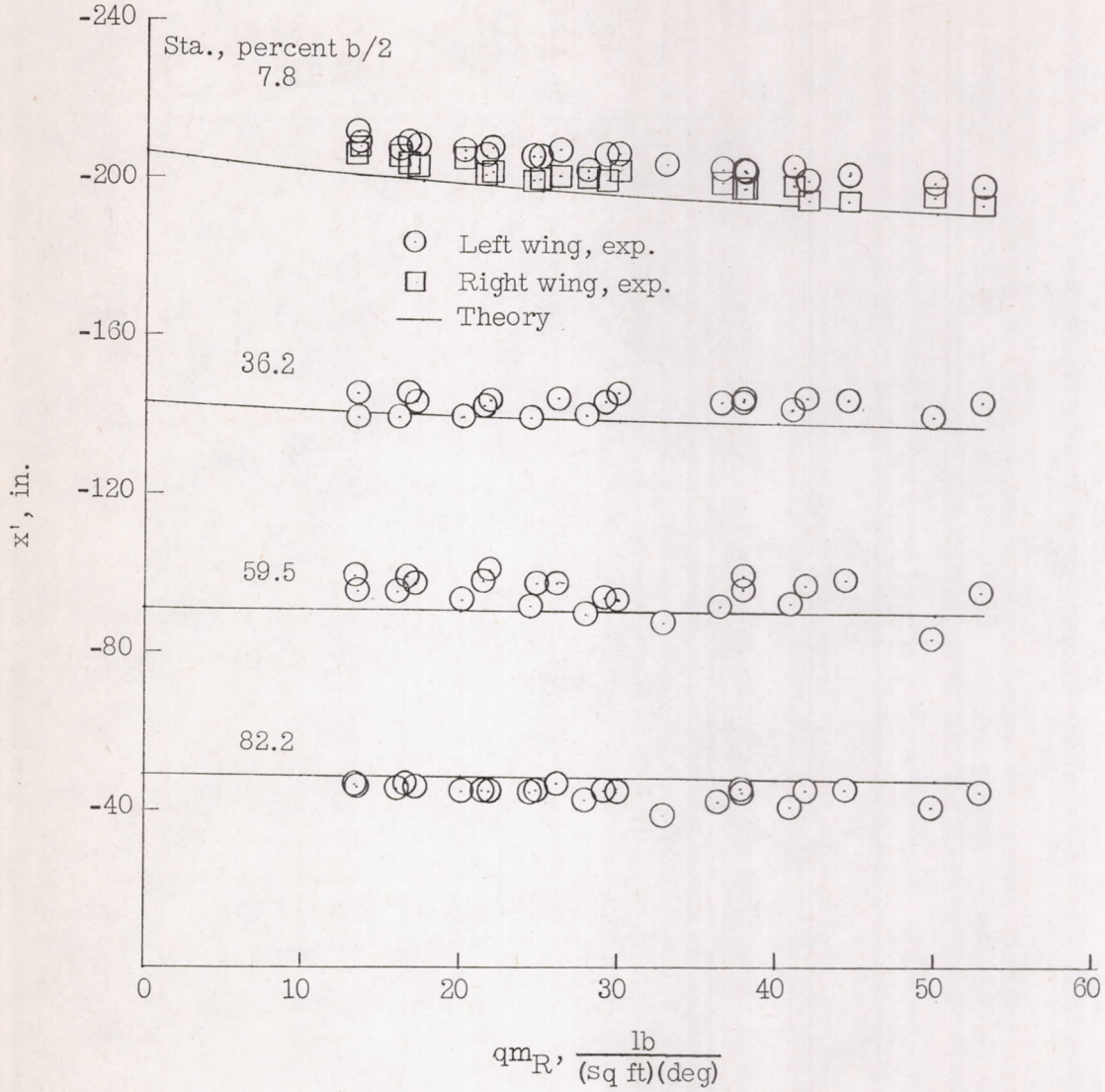

(b) Streamwise coordinates.

Figure 5.- Concluded.

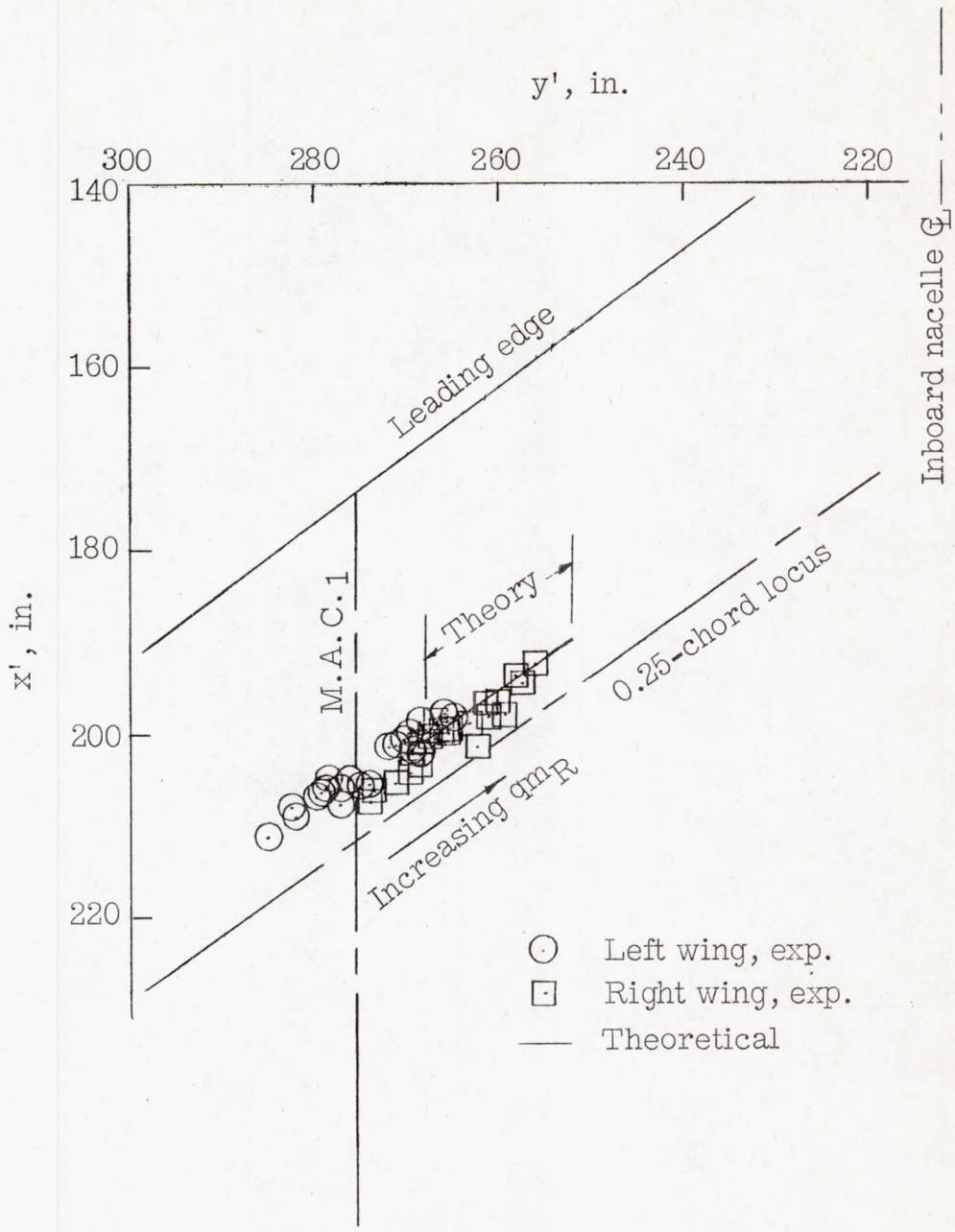

Figure 6.- Experimental and theoretical locations of additional-airload center of pressure with respect to quarter-chord locus and mean aerodynamic chord for area outboard of 7.8 percent semispan.

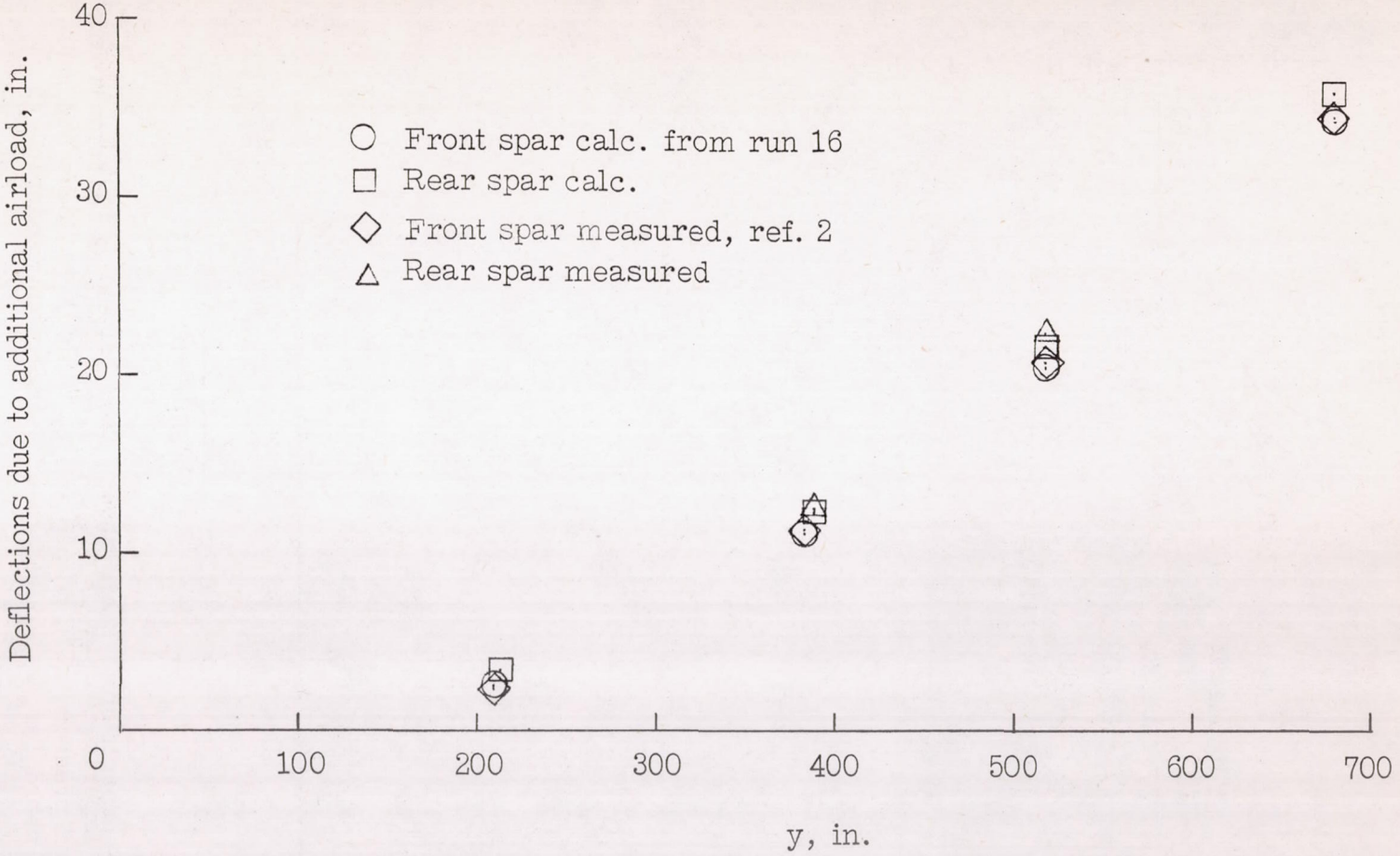

Figure 7.- Wing deflections calculated from measured additional airload shears compared with measured deflections from reference 2. Measured rear-spar deflections not available at y = 212 and 681.

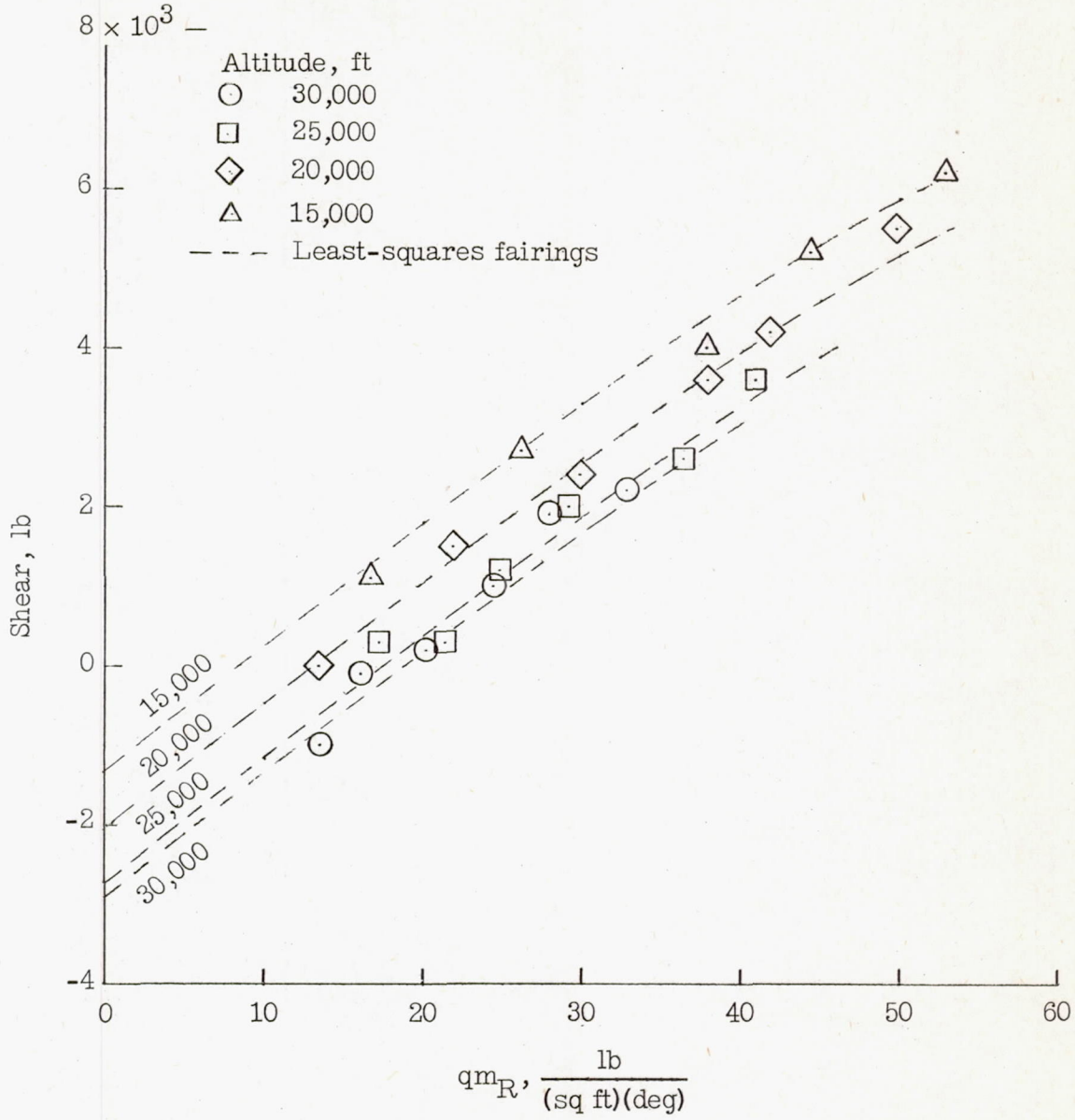

Figure 8.- Experimental basic shears from left-wing root measurements illustrating zero shifts.

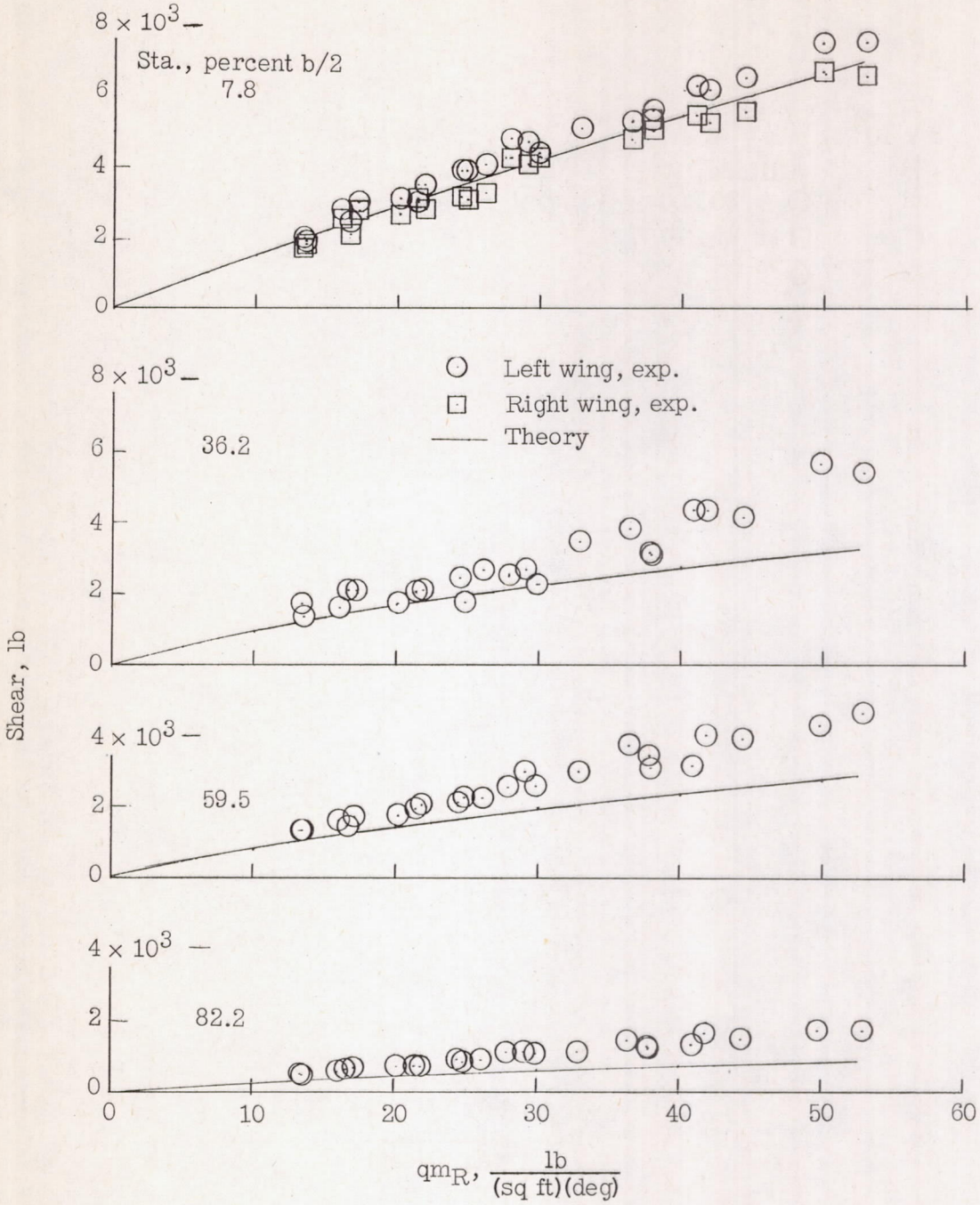

(a) Basic shears.

Figure 9.- Adjusted basic loads at each strain-gage station in comparison with predicted basic loads.

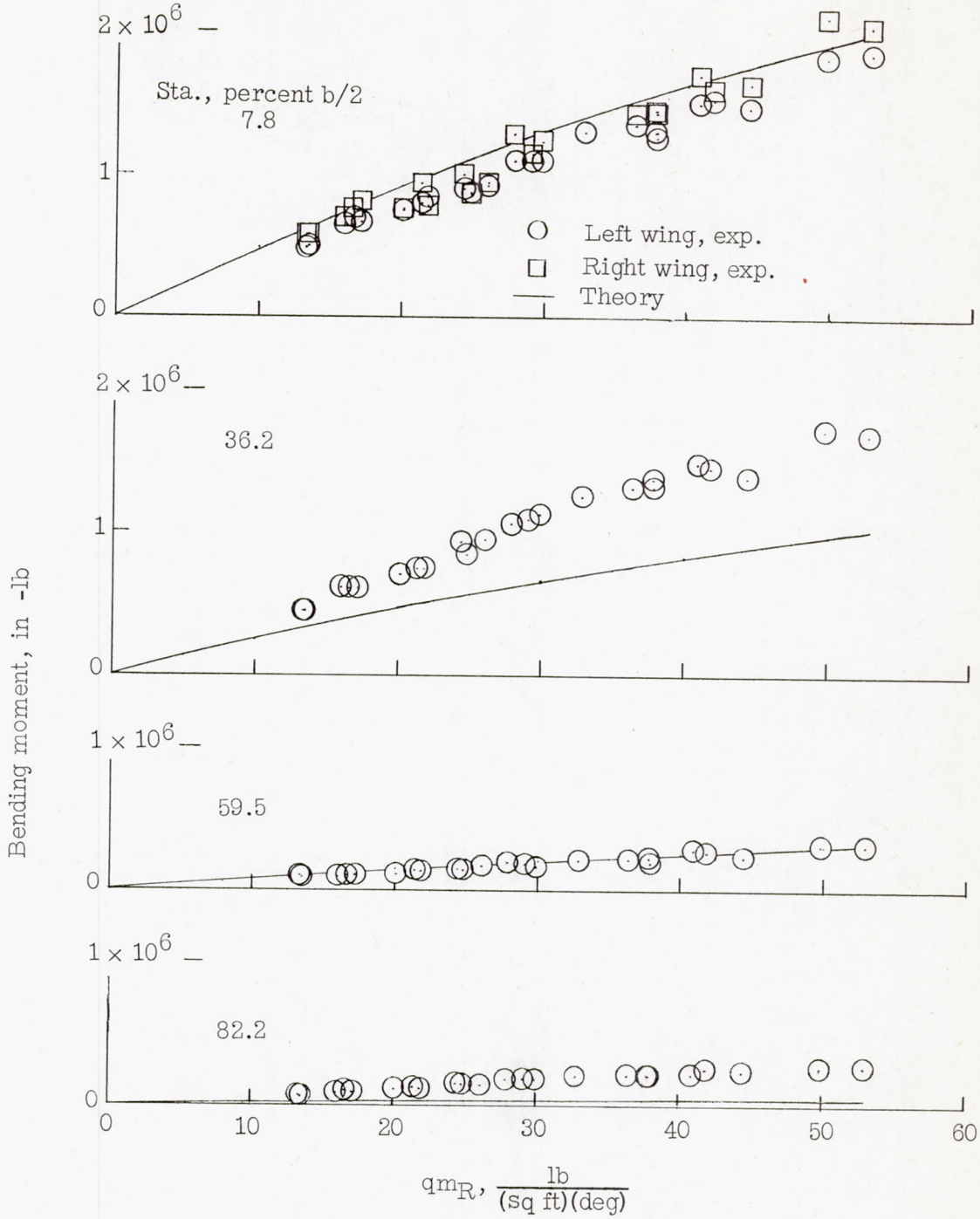

(b) Basic bending moments.

Figure 9.- Continued.

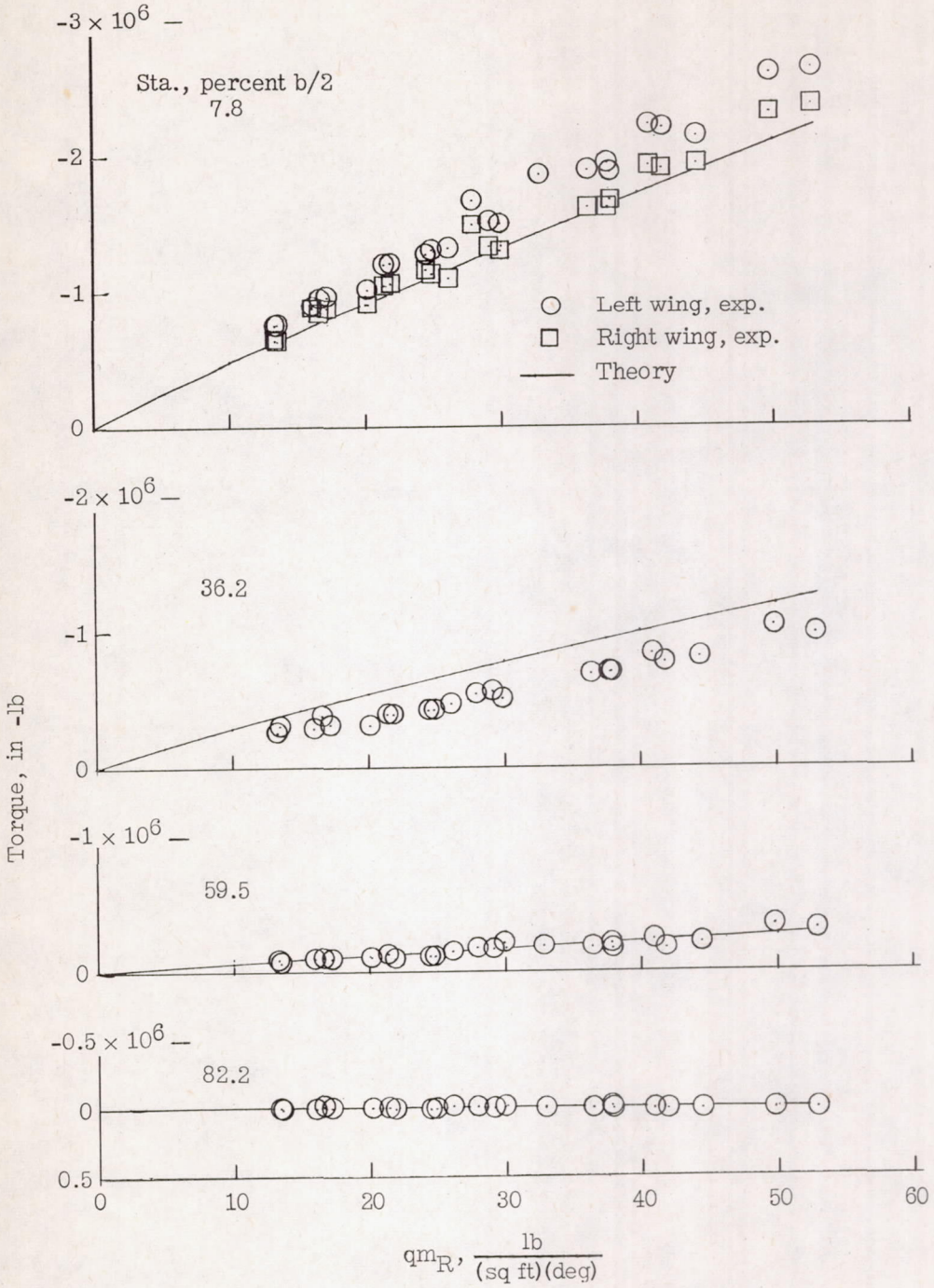

(c) Basic torques.

Figure 9.- Concluded.